Testing of NMC and LFP li-ion cells for surface temperature at various conditions

Ognjen Popović, Veljko Rupar, Željko Praštalo, Snežana Aleksandrović, Vladimir Milisavljević

Testing of NMC and LFP li-ion cells for surface temperature at various conditions | Ognjen Popović, Veljko Rupar, Željko Praštalo, Snežana Aleksandrović, Vladimir Milisavljević | Case Studies in Thermal Engineering | 2024 | |

10.1016/j.csite.2024.104930

http://dr.rgf.bg.ac.rs/s/repo/item/0009389

Case Studies in Thermal Engineering 61 (2024) 104930

Contents lists available at ScienceDirect

Case Studies in Thermal Engineering

journal homepage: www.elsevier.com/locate/csite

Testing of NMC and LFP Li-ION cells for surface temperature at various conditions

Ognjen Popović [a, *], Veljko Rupar [b], Željko Praštalo [a], Snežana Aleksandrović [b], Vladimir Milisavljević [b, **]

[a] *Mining Institute Belgrade, Serbia*
[b] *University of Belgrade, Faculty of Mining and Geology, Belgrade, Serbia*

ARTICLE INFO

Handling Editor: Dr Y Su

Keywords:
Battery electric vehicles
Heat load
Li-ion cells
NMC
LFP
Cell's surface temperature

ABSTRACT

Battery electric vehicles (BEVs) are being considered as a replacement technology for diesel vehicles in underground mining of mineral resources. However, many issues related to BEVs in industrial applications still require more detailed research. One significant topic is the heat load—BEVs' heat emission into the working environment during regular operation. This paper provides an overview of the thermal behavior of NMC and LFP Li-ion cells tested under various conditions, which is an important step in determining the overall heat load of BEVs. The surface temperature of three NMC and one LFP 18650 Li-ion cells was monitored during charging and discharging at four different rates, at constant ambient temperatures of 30 °C and 40 °C. The main results pertain to the cell's thermal behavior during charging and discharging, highlighting the distinctive temperature profiles of NMC and LFP cells.

1. Introduction

Battery electric vehicles (BEVs) with lithium-ion batteries are becoming common technology in the underground mining of mineral deposits. While the current number of these machines is not high, it is expected that they will become an alternative and more relevant choice compared to diesel machines.

As stated in professional literature [1], there are currently 157 electric loaders and 45 electric trucks operating in underground mines worldwide. Original equipment manufacturers refer to such information on their own portals, projects, and publications [2–4].

The application of BEVs in underground mines has a less harmful impact on the working environment because they do not consume oxygen and do not emit exhaust gases [5]. Electric motors emit less noise, and their efficiency is over 90 %, resulting in minimal heat emission [6]. Additionally, electric powertrains and transmissions are less complicated, making their usage and maintenance simpler. These attributes highlight the advantages of BEVs, which contribute to their increasing prevalence.

The application of these machines is justified by their reduction of exhaust gases, decreased heat load, and overall contribution to the mitigation of greenhouse gas (GHG) emissions. However, a notable disadvantage of these vehicles is their limited operational time per battery charge. Consequently, batteries must be recharged or replaced frequently, depending on their type and capacity. Nonetheless, substantial research is being conducted in this area, leading to significant advancements. As a result, it is anticipated that the characteristics of batteries, such as vehicle range and battery capacity, will continue to improve[7,8].

* Corresponding author.
** Corresponding author.
E-mail addresses: ognjen.popovic@ribeograd.ac.rs (O. Popović), vladimir.milisavljevic@rgf.bg.ac.rs (V. Milisavljević).

https://doi.org/10.1016/j.csite.2024.104930
Received 21 March 2024; Received in revised form 5 June 2024; Accepted 3 August 2024
Available online 5 August 2024

With the increasing depth of underground mines and higher production rates, greater demands are placed on vehicle routes for main haulage. Consequently, higher mine production leads to increased air pollution [9]. Additionally, as depth increases, the temperature of the working environment also rises [10]. For example, in the world's deepest mine in South Africa, temperatures can reach 55 °C [11].

Li-ion batteries (LIBs) have had a significant impact on the development of electric vehicles [12], including industrial vehicles used in mining mobile mechanization. The primary technological concerns regarding this technology involve the safe use of lithium-ion batteries, their thermal stability, fast charging, and performance improvement at low and high temperatures. Research on the thermal performance of lithium-ion batteries [13–16] indicates the necessity of optimizing their thermal performance and thermal management systems in accordance with energy density and charge rate. However, LIBs generate a considerable amount of heat during the charging and discharging process, and if heat dissipation is insufficient, it can lead to an increase in cell pack temperature, causing capacity decay and performance degradation [17].

Additionally, it is important to maintain effective monitoring and management of the battery state [18], including the regenerative braking function [19]. Economic factors are also significant, such as the capital expenses for acquiring such equipment with batteries, as well as operational expenses [20,21].

Another important issue is understanding the heat generation and heat transfer processes. Recent research is focused on the behavior of systems for thermal management of batteries [22], the regulation of thermal phenomena within the battery itself [23,24], and developing methodologies for assessing the temperatures within the battery during charging and discharging [25].

However, the specifics of underground mining necessitate a comprehensive understanding of heat emission into the working environment during regular operation—known as heat load. This topic is elaborated in detail by M. J. McPhearson [26], but BEVs with Li-ion cells are a recent technology in this context.

Given the importance of heat transfer analysis in underground mining, experimental research on this subject has commenced at the University of Belgrade, Faculty of Mining and Geology. The main goal of the research is to determine the amount of energy emitted from BEVs into the working environment of underground mines in the form of heat.

The focus of this paper is on the results of Li-ion cell surface temperature measurements under various charging and discharging rates at different temperatures. These results will be used in subsequent steps to establish the heat load.

2. Testing method and setup

Four Li-ion cells were tested in total, of which three are NMC (nickel-manganese-cobalt) and one is LFP (lithium ferro-phosphate). Currently, NMC cells have a larger energy density, while LFP cells are considered to be more stable. The research presented in this paper was conducted on 18650 cells. These cells are cylindrical in shape, with a length of 65.2 mm and a diameter of 18.6 mm, enclosed in a plastic-covered steel casing. The specifications of the cells used in the tests, according to the manufacturers, are provided in Table 1.

All tests were performed in a thermal chamber (Colo DRYSC 136, forced air convection oven), with preheating of the cells until they stabilized at the ambient temperature, generally taking 90–120 min. The cell surface temperature was also monitored during the preheating stage to ensure that any temperature variation in the cell was caused by reactions within the cell and not by differences in ambient temperature.

During the tests, the temperature on the surface of the cell was measured using a type J (Fe) thermocouple, while the ambient temperature was measured using a type K (Ni-Cr) thermocouple. The thermocouples were connected to and recorded by a Testo 175T3 temperature data logger, with accuracy of ± 0.5 °C $\pm$ 1 digit. Additionally, the voltage of the cells was measured directly at the terminals using a Fluke V3001FC voltmeter, with accuracy of ± 0.09 % + 3 digits. The charger used was a Siglent SPD 3303C, and the load was a Siglent 1000X. Accuracy of Siglent instruments is ± 0.5 % + 1 digit, both for voltage and current. Temperature measurements were taken at 10-s intervals, while voltage measurements were taken at 1-s intervals. The complete setup is shown in Fig. 1, and the scheme is shown in Fig. 2.

All cells were charged with their nominal charge voltage (4.2 V for NMC cells and 3.65 V for LFP cells), and then discharged to a voltage of 2.7 V. It is important to note that the charger and the load have the capability to record voltage during these processes. However, the measurement results presented are from a Fluke voltmeter, which is connected directly to the cell terminals, thereby avoiding voltage drops in the setup wiring.

The tests were done systematically, with constant current. The cells were charged and discharged at rates of 1C, 0.75C, 0.5C and 0.33C[1] at ambient temperatures 30 °C and 40 °C. In total, 64 tests were performed.

3. Results and analysis

The graphs in this chapter are showing the changes in the voltage and the surface temperature of cells during charging and discharging processes, at constant environment temperature.

[1] Symbol "C" stands for C rate, value used for expressing the speed of cell charging or discharging. The unit of the C rate is Ampere-Hour (Ah). The value of 1C means that the cell or a battery is charged/discharged in 1 h. Consequently, 0.5C and 0.33C rates are standing for currents used for charging/discharging the cell in 2 and 3 h respectively. The C rate is used for testing cells of different capacities during charging and discharging in same time interval. Consider the fully charged cell with capacity of 2500 mAh (2.5 Ah). To achieve discharge rate of 1C, the load current should be 2500 mA and resulting in fully discharged cell in 1 h. For discharge rates 0.5C and 0.33C the load currents should be 1250 mA and 833 mA, resulting in fully discharged cell in 2 and 3 h respectively.

Table 1
Specification of tested cells.

Characteristic/cell	P26A	VTC5A	25R	Heter
Type	NMC	NMC	NMC	LFP
Capacity (mAh)	2600	2500	2500	1400
Nominal voltage (V)	3.6	3.6	3.6	3.2
Charge voltage (V)	4.2	4.2	4.2	3.65
Discharge voltage (V)	2.5	2.5	2.5	2.5
Charge current (A), max	6	6	6	4.2
Discharge current (A), max	35	35	35	4.2

Fig. 1. Experiment setup (thermal chamber, electric load, power supply and voltmeter).

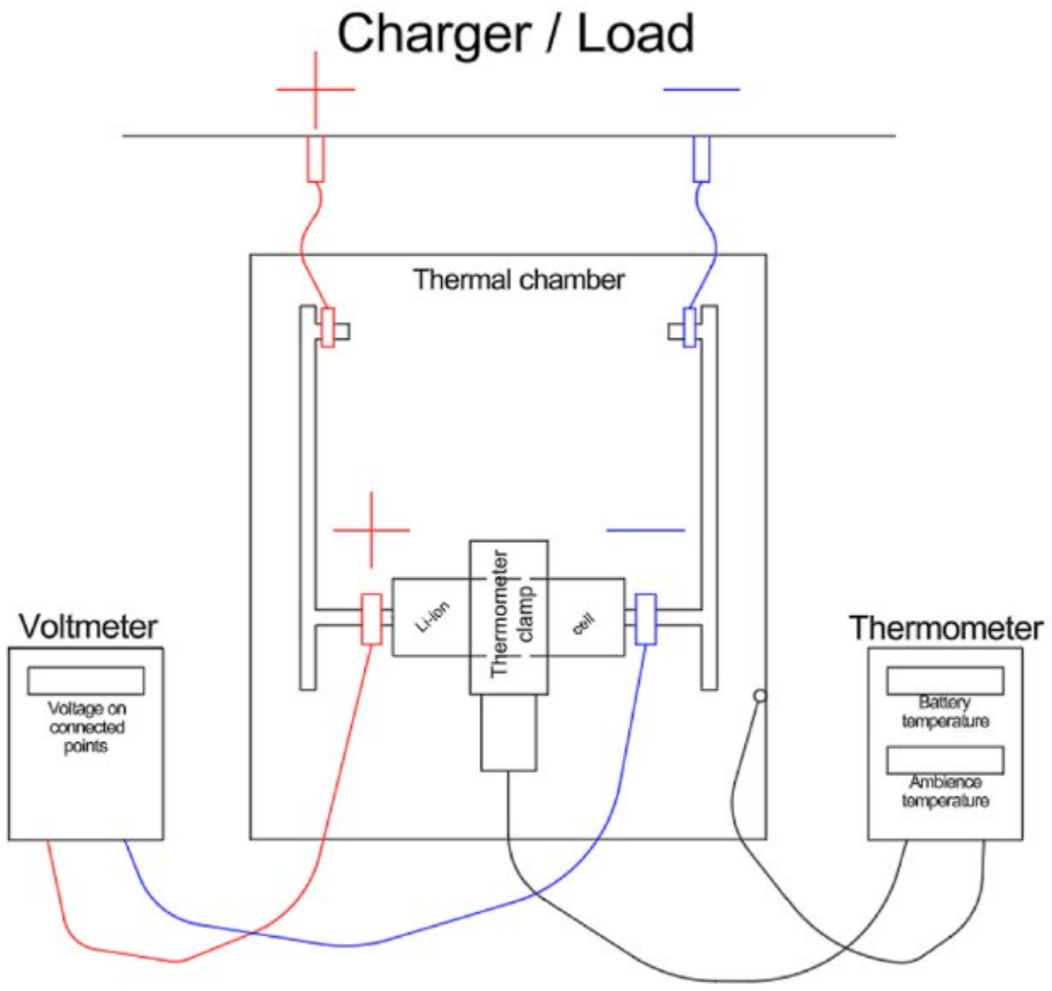

Fig. 2. Technical scheme of mentioned equipment.

Voltages and surface temperatures variation during charging of all cells with 0.33C, 0.5C, 0.75C and 1C rates at 30 °C ambient temperature is shown on Fig. 3.

As can be seen, there are 4 data sets of voltage and 4 data sets of temperature, one for each cell. The left vertical axis indicates the voltage, shown in the upper part of the graph. The right vertical axis indicates the temperature, and the horizontal axis represents time, in seconds. Bottom legend provides color code of voltage (U) and temperature (t) for different cells.

The tests show that charging time is closer to the theoretical one while charging with lower current. At 0.33C charging rate (Fig. 3a) three NMC cells have almost identical charging time, while the LFP cell has slightly shorter charging time. The actual charging time for NMC cells is about 10000 s, or 2 h and 46 min. With 0.5C charging rate (Fig. 3b) all the tests of NMC cells lasted for about 7000 s, while this time for LFP cell was around 6000 s. Fig. 3c (charging rate 0.75C) shows charging times of about 4100–4200 s for LFP and NMC P26A cells and over 5000 s for other two NMC cells. As shown on Fig. 3d the charging periods are shorter than expected (60 min), by 7–15 min at 1C rate.

Voltage trends of the NMC cells are almost linear, excluding the beginning and the end of the tests, while the LFP cell showed smaller change during the test, again, excluding the beginning and the end. Voltage graphs are similar in all tests, but slight distinctions occur for NMC cells during charging at 1C rate (Fig. 3d). The starting voltages of NMC cells are somewhat different, due to different storage periods and consequent self-discharge, but within several minutes this effect is neutralized. Recharging of the cells prior to the test was avoided to exclude any remaining heat from the charging process.

Cells surface temperature change during charging at 0.33C rate is minor. As it can be seen on Fig. 3a, the temperature reaches its maximum at the very end of the test, but the trend is not linear and does not rise throughout the test. It reaches local maximum during the first third to half of test, then it drops, followed by the second maximum toward the end of the test.

Similar behavior was observed during charging with 0.5C rate (Fig. 3b), with somewhat sharper changes. In this case, all NMC cells are demonstrating two local maximums, as well as temperature rise toward the end of the test. In this case, the temperature peak is on the second maximum, not at the end as in the previous case. LFP cell had only one surface temperature maximum and the peak temperature at the end, as in previous case.

Surface temperatures graphs for NMC cells, at charging rate of 0.75C (Fig. 3c), indicate just one local maximum during the second part of the test interval, with the period of somewhat constant temperature (plateau) in the first part. Temperature profile of the LFP cell is similar to the previous tests.

Surface temperatures variations are the most rapid for NMC cells at charging rate 1C, as shown on Fig. 3d. Also, in this case LFP cell is not heating up as much as the NMC cells. This test clearly shows that the temperature maximum for NMC cells is reached before the end of the charging process, while the maximum temperature of LFP cell is achieved at the end of test. It should be noted that all charging graphs show a slight drop of LFP surface temperature at the beginning of tests, but it quickly recovers and starts rising. Profiles of surface temperature graphs for NMC cells are also following previously mentioned pattern, initial rapid increase followed by the plateau and toward the end of the test, slight temperature increase with the maximum and at the end very low drop of tempera-

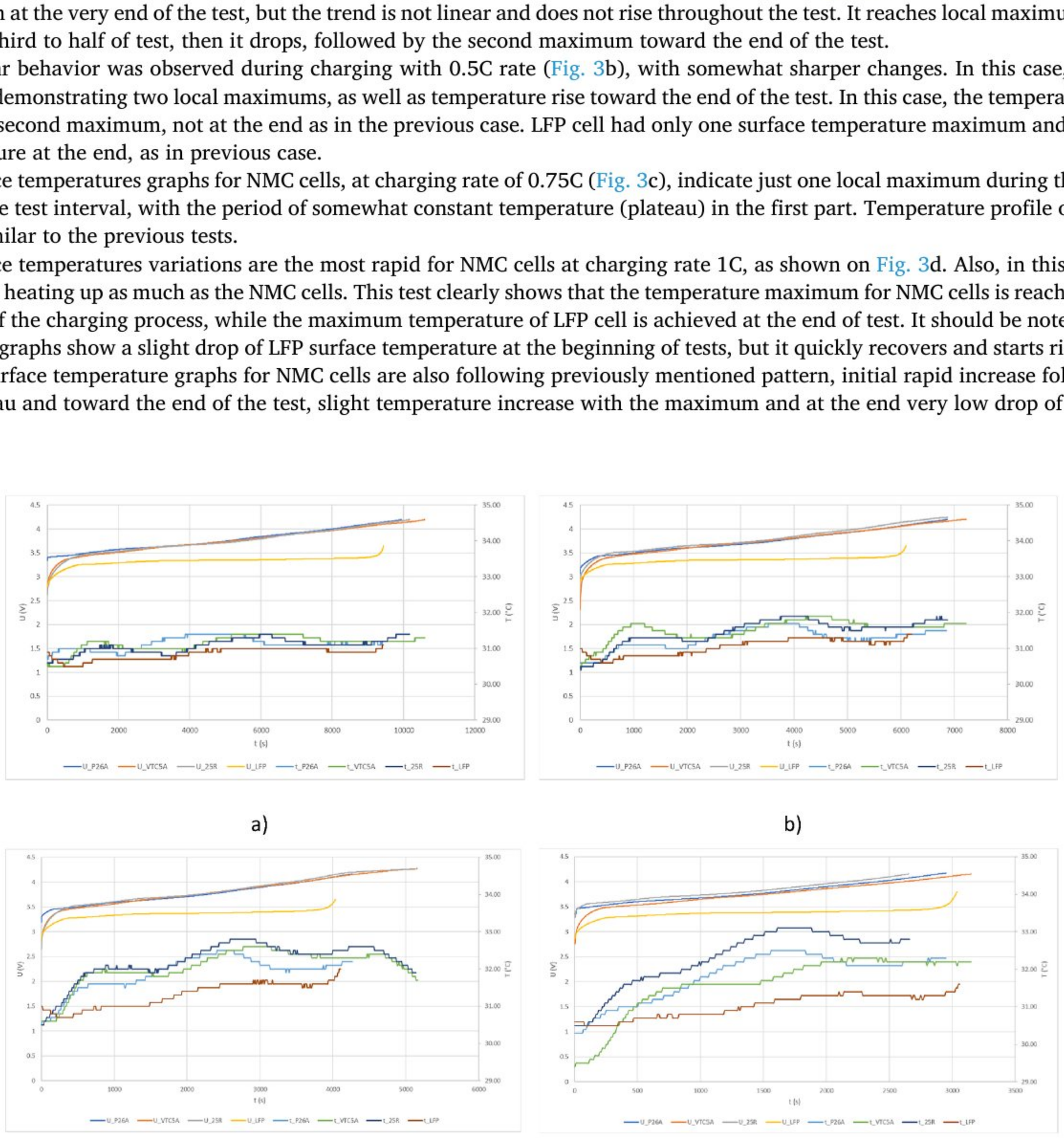

Fig. 3. Voltage and surface temperature of cells during charging at 30 °C ambient temperature a) 0.33C, b) 0.5C, c) 0.75C, d) 1C.

ture. With the higher current, the NMC cells graphs of surface temperature variations are more dispersed – achieving different temperatures, depending on the cell model (comparing 0.33C graph with 1C graph).

Voltages and surface temperatures variations during discharging of all cells with 0.33C, 0.5C, 0.75C and 1C rates at 30 °C environment temperature is shown on Fig. 4.

Discharging tests periods at all rates (Fig. 4) are very similar to the charging periods.

As seen on Fig. 4 the NMC cells have linear voltage drop throughout the test with more rapid drop at the end with more dispersed voltage variations. The LFP cell has the pattern opposite to the charging process, with slight voltage drops at the beginning and more significant at the end of the test. This behavior corresponds to the specifications and properties for this type of Li-ion cells.

The temperature variations while discharging at 0.33C rate, shown on Fig. 4a, are small with an increasing trend at the end of tests and this corresponds to the rapid decrease of voltage. The 0.5C charging rate curves (Fig. 4b) are similar to previous one, but it clearly indicates that temperature of LFP cell does not increase as rapidly as the surface temperatures of NMC cells at the end of tests. Also, it is evident that there is a temperature local maximum during the first half of tests followed by slight drop, just to rise again and reach its maximum at the end. At 0.75C charging rate the temperature curves (Fig. 4c) are more distinctive and the first local maximum is more evident. It is also visible that some cells have periods with somewhat constant surface temperature during the middle of the test before it rapidly increases and reaches maximum at the very end. During charging with 1C rate the temperature curves, shown on Fig. 4d, are almost completely distinctive for each cell and it is obvious that temperature of LFP is not increasing as much as the NMC cells. The surface temperature of the LFP cell remained almost constant at the beginning of the test before it started incremental rise – this behavior is typical for this type of Li-ion cells.

Voltage and surface temperatures variations during charging of all cells with 0.33C, 0.5C, 0.75C and 1C rates at 40 °C environment temperature is shown on Fig. 5.

This test is performed in the same conditions as the previous one, shown in Fig. 3, except for ambient temperature which was 40 °C. The charging time at 0.33C and 0.5C rates are similar when compared to the charging at 30 °C ambient temperature at same rates. However, charging at 0.75C and 1C was performed in shorter period.

The trends of the voltage curves are identical to the same tests performed at lower temperature, meaning that ambient temperatures within these limits are having no impact on cell's voltage.

It can also be seen that charging at 0.33C rate have surface temperature variations (Fig. 5a) remarkably similar as in test on 30 °C, with slightly more distinction between the NMC cells.

At 0.5C charging rate (Fig. 5b), NMC cells again are having visible local maximums of surface temperature, first at the beginning of the test and the second in the latter half of the test. The first temperature maximum of the NMC cells comes after sharper temperature increase in brief time, and it is at lower value than the second maximum which appears after more gradual temperature increase during longer period.

Profile of temperature curves of NMC cells, during charging at 0.75C and 1C (Fig. 5c and d) are similar and comparable to those obtained at 30 °C ambient temperature. However, the first maximum is less pronounced i.e., "flattened", meaning that surface temperature of the NMC cells is constant or stagnating after initial period of temperature rise. This period is followed by the second tem-

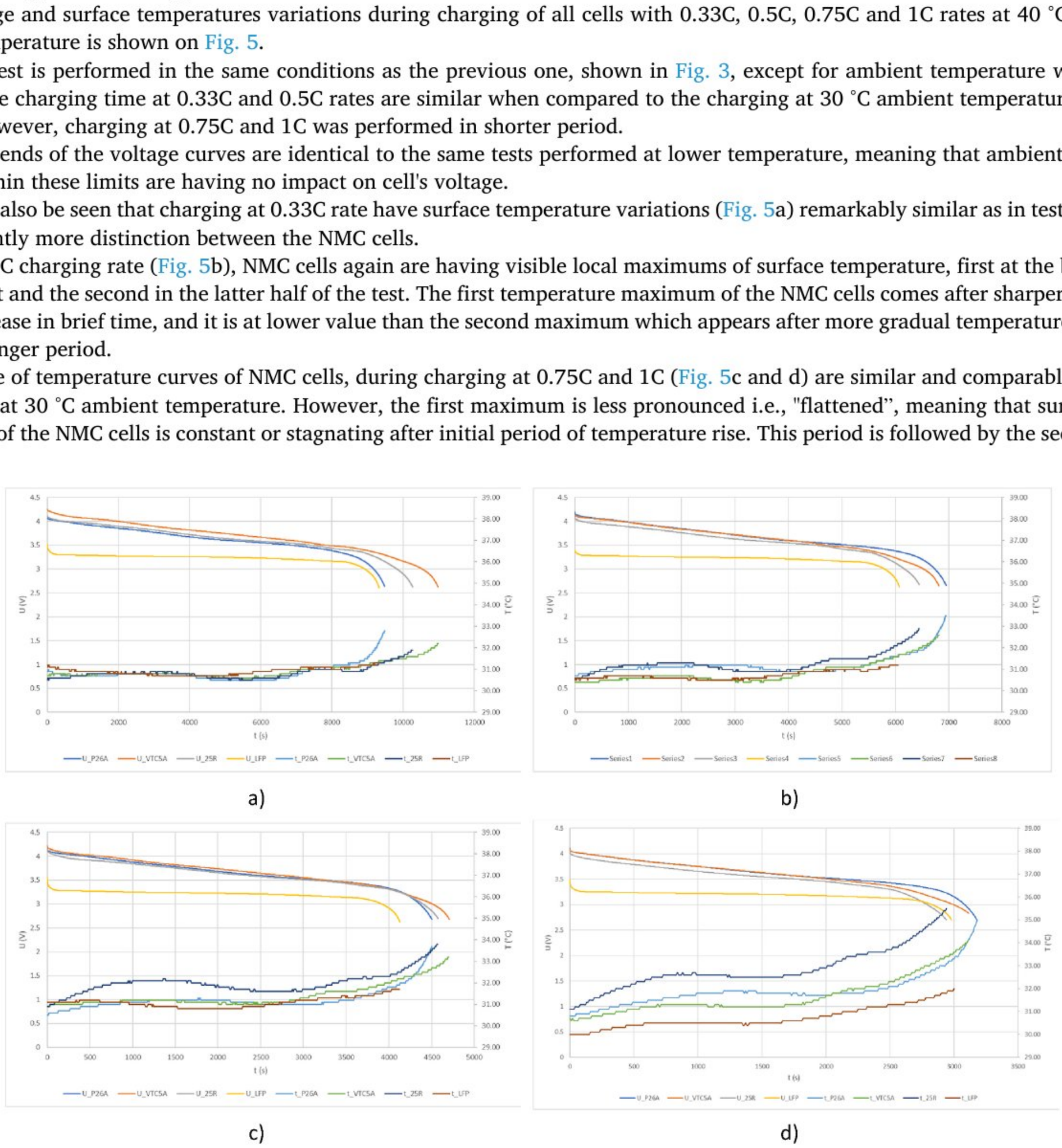

Fig. 4. Voltage and surface temperature of cells during discharging at 30 °C ambient temperature a) 0.33C, b) 0.5C, c) 0.75C, d) 1C.

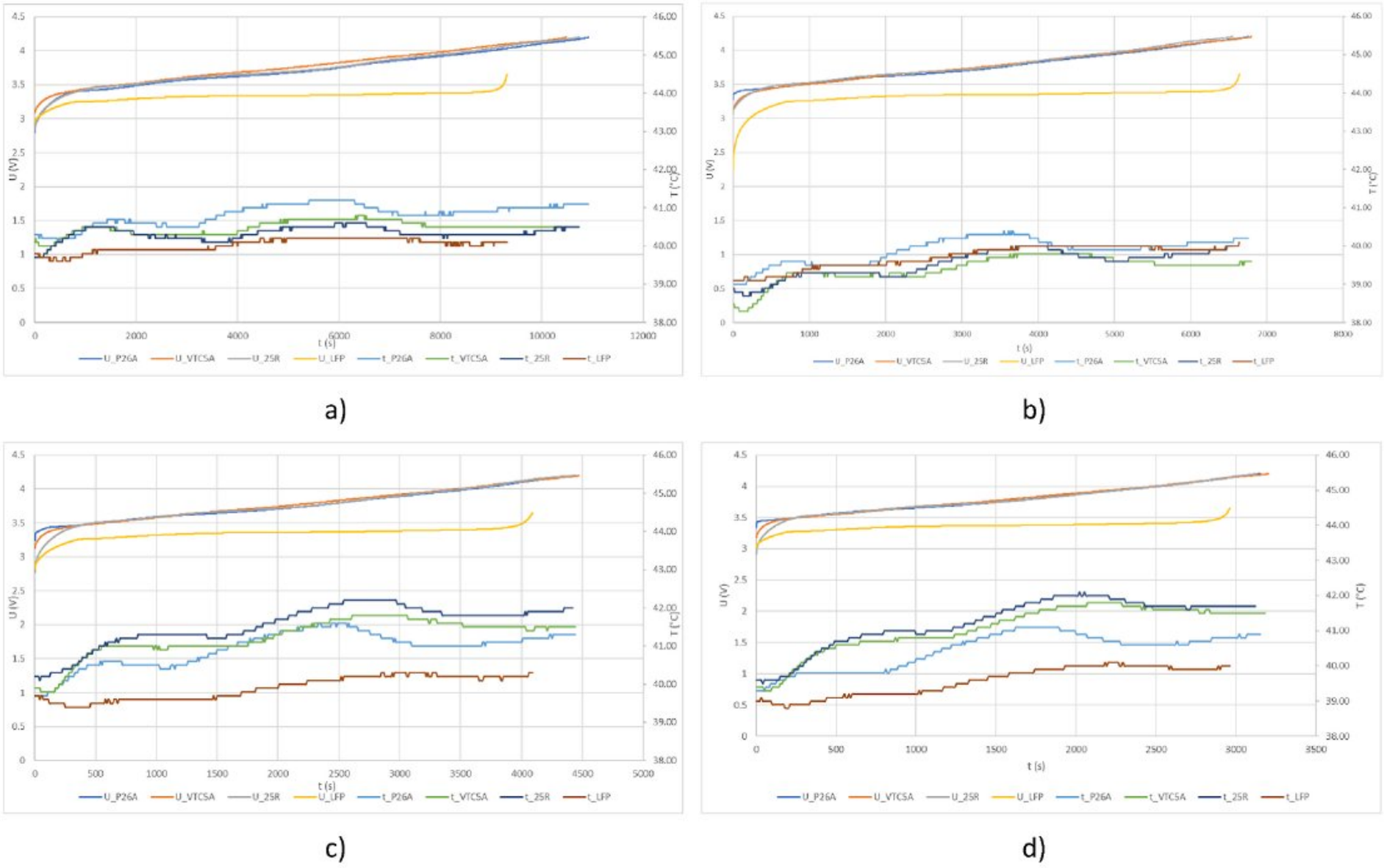

Fig. 5. Voltage and surface temperature of cells during charging at 40 °C ambient temperature a) 0.33C, b) 0.5C, c) 0.75C, d) 1C.

perature rise and maximum in the second half of the test. Again, surface temperature of the NMC cells is higher in comparison to the LFP cell. The LFP cell also reaches the maximum temperature during the second half of the test, followed by negligible drop toward the end.

Similar observations made for the charging test performed at 30 °C ambient temperature is applicable for this test.

Voltages and surfaces temperatures variations during discharging of all cells with 0.33C, 0.5C, 0.75C and 1C rates at 40 °C environment temperature are shown on Fig. 6.

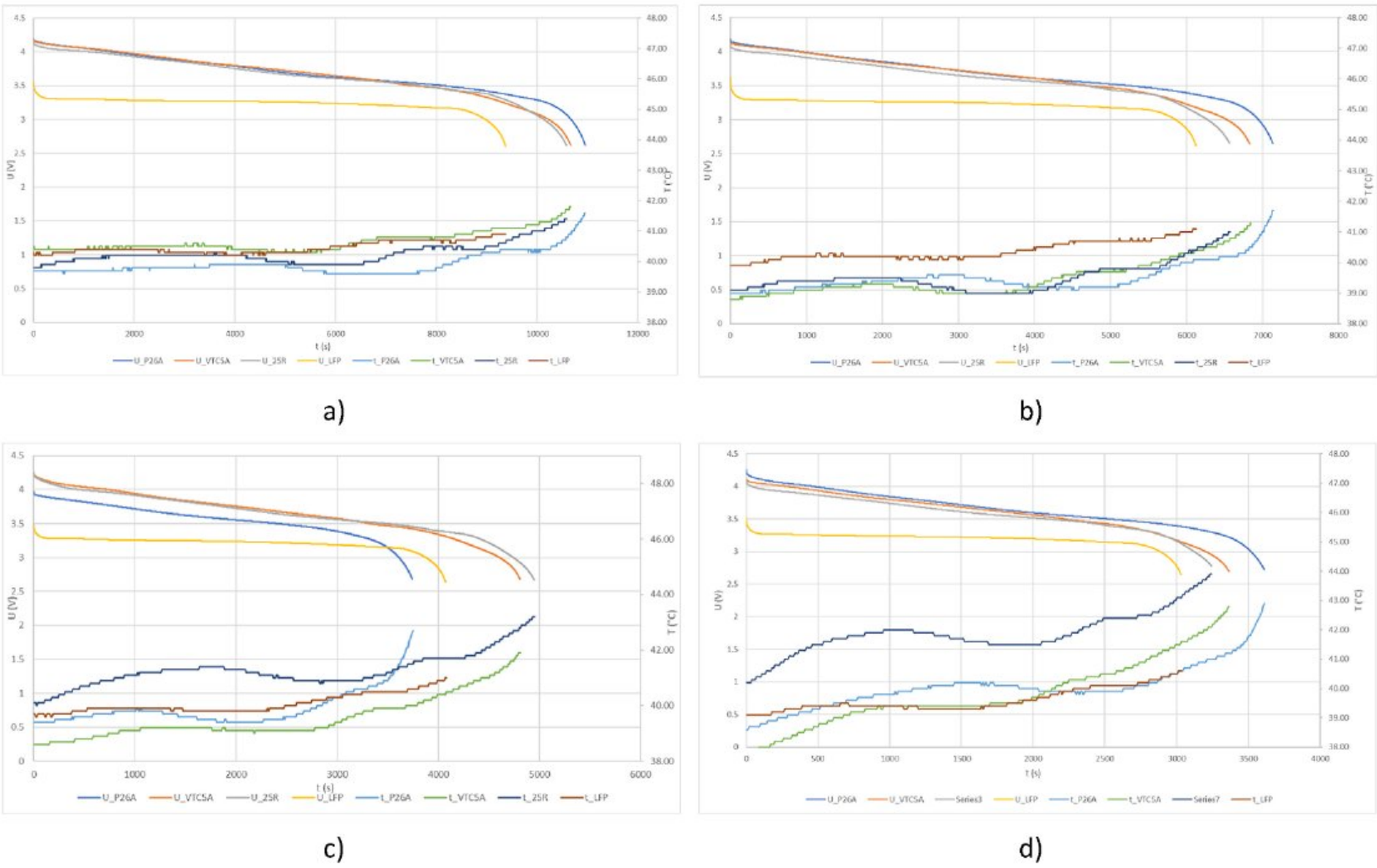

Fig. 6. Voltage and surface temperature of cells during discharging at 40 °C ambient temperature a) 0.33C, b) 0.5C, c) 0.75C, d) 1C.

Similar graphs patterns of this test were observed in comparison to the test performed at 30 °C, regarding discharging time and voltage drop. However, the discharging period of NMC cells was longer at higher rates (0.75C and 1C – Fig. 5c and d) by 10–15 %, when compared to same tests at 30 °C (Fig. 4c and d).

Surface temperature of all cells at lower discharging rates (Fig. 6a and b) are following the same trend as in previous test, but with more distinctive periods of heating and cooling for NMC cells. Again, surface temperature of all cells shows rapid increase at the end of tests and the start of this corresponds to the rapid decrease of voltage.

At 0.75C charging rate the temperature curves of each cell are more distinctive, as shown on Fig. 6c. NMC cell P26A was discharged faster due to voltage drop during the storage period. Even larger distinction of surface temperature curves is evident during charging at 1C rate, shown on Fig. 6d.

LFP cell did not demonstrate any distinction between the tests performed at 30 °C and 40 °C ambient temperature.

Other observations made for the rest of cells tested at 30 °C are valid for this test.

4. Discussion and conclusions

The purpose of the tests described above is to determine the behavior of Li-ion cells during discharge and charging under various conditions, with a focus on surface temperature.

Table 2 provides the relative maximum values of temperature rise (ΔT), which is the increase from the initial to the maximum temperature for each tested cell.

It is evident that the measured temperature variations are higher during cell discharging process for NMC cells, while surface temperature of LFP cell are more consistent. Also, NMC cells are having higher temperature peaks, when compared to the LFP cell. This corresponds to description of LFP cells as more stable cells. It can also be seen that the peaks are higher with higher rates of charging and discharging.

As it can be seen, there is no significant distinction between results obtained at 30 °C and 40 °C ambient temperatures for P26A and 25R NMC cells. The VTC5 showed higher surface temperatures at 40 °C ambient temperature during charging at 0.5C, 0.75C and 1C. LFP cell, Heter, also had higher surface temperatures at 40 °C ambient temperature, except for the highest charging rate. However, this needs to be confirmed by further research.

It is known that there are two heat sources in a cell: Joule's or Ohmic heating and entropy change due to electrochemical reactions. Joule's or Ohmic heating is defined by:

$$\dot{Q} = I\left(E - V_a\right) - I\left[T\left(\frac{dE}{dT}\right)\right] \tag{1}$$

Where.

$\dot{Q}$ – Heat generation rate (Ws);
I – Current (A);
E – Open circuit voltage (V);
V_a – Cell voltage (V);
T – Temperature (C);
$\frac{dE}{dT}$ – Temperature coefficient (V/C).

The first term is known as Joule's heating and the I•[T•(dE/dT)] is reversible heat from open circuit voltage changes due to temperature at electrodes. Usually, the second term is small compared to the first term and can be neglected, for current rates of BEVs [27,28]. The first term can be considered as a constant, meaning that all the variations of the surface temperature are caused by the electrochemical reactions inside the cell.

Table 2
Temperature differences (ΔT) for tested cells.

Current rate	30 °C				40 °C			
	0.33C	0.50C	0.75C	1C	0.33C	0.50C	0.75C	1C
Cell	P26A							
Discharging	1.9	2.8	3.2	4.2	1.9	2.7	3.3	4.3
Charging	0.6	1.1	2	2.2	0.9	1.4	1.9	1.8
Cell	VTC5A							
Discharging	1.5	2.2	2.3	3.4	1.4	2.5	3.3	4.9
Charging	0.8	1.4	2	2.9	0.7	1.3	1.9	2.4
Cell	25R							
Discharging	1.4	2.3	2.9	4.4	1.6	1.9	3.1	3.7
Charging	0.8	1.4	2.3	2.6	0.9	1.1	2	2.5
Cell	Heter							
Discharging	0.1	0.7	0.6	2	0.6	1.2	1.3	1.5
Charging	0.2	0.4	1	1	0.4	1	0.6	1.1

These electrochemical reactions occur in intervals shorter than the charging and discharging cycles of the cells and can be exothermic or endothermic, directly depending on the compounds used to create the anode, cathode, and electrolyte. Therefore, these reactions contribute to variations in the surface temperature of the cell.

Additionally, it is evident that these reactions cause differences between NMC and LFP cells, as well as varying profiles among the NMC cells. LFP cells exhibit a consistent temperature rise throughout the entire test. In contrast, NMC cells experience periods of decreasing surface temperature, occurring at different times for different cells. It is evident that a higher surface temperature of the cell results in greater heat generation.

Presented results are important for future research related to the heat load of battery electric vehicles in underground mines. Next step comprises of further testing of Li-ion cells related to heat generation parameters and modelling of heat emissions, i.e., heat load of the BEV's to the underground mining working environment. This is to be achieved by correlating the measured surface temperatures with the heat generation rate, as described in Equation (1).

CRediT authorship contribution statement

Ognjen Popović: Writing – review & editing, Writing – original draft, Visualization, Methodology, Formal analysis, Data curation, Conceptualization. **Veljko Rupar:** Validation, Resources. **Željko Praštalo:** Resources, Project administration, Investigation, Formal analysis. **Snežana Aleksandrović:** Writing – review & editing, Project administration, Formal analysis. **Vladimir Milisavljević:** Writing – review & editing, Writing – original draft, Validation, Supervision, Methodology, Investigation, Conceptualization.

Declaration of competing interest

The authors declare that they have no known competing financial interests or personal relationships that could have appeared to influence the work reported in this paper.

Data availability

Data will be made available on request.

References

[1] Miners continue to expand use of battery-powered vehicles underground, J. Mining Technology (2022). https://www.mining-technology.com/comment/battery-powered-underground/.
[2] International mining, https://im-mining.com/tag/minetruck-mt42-battery/. (Accessed 26 February 2024).
[3] Sandvik Press Release, Sandvik Wins Record SEK 330 Million Order for Battery-Electric Mining Equipment, 2022.
[4] M. Hatton, W. Lewis, L. Jones, J. Howery, M. Franceschini, A. McIntyre, K. Kalenchuk, Technical Report on the Feasibility Study for the McIlvena Bay Project, Saskatchewan Canada, 2022, pp. 17–394.
[5] A. Fugiel, D. Burchart-Korol, K. Czaplicka-Kolarz, A. Smoliński, Environmental impact and damage categories caused by air pollution emissions from mining and quarrying sectors of European countries, J. Clean. Prod. 143 (2017) 159–168.
[6] B. Lukasz, Global Trends in the Development of battery-powered underground mining machines, Multidisciplinary Aspects of Production Engineering 4 (1) (2021) 178–189.
[7] C. Iclodean, B. Varga, N. Burnete, D. Cimerdean, Jurchiş, Comparison of different battery types for electric vehicles, IOP Conf. Ser. Mater. Sci. Eng. 252 (2017) 012058, https://doi.org/10.1088/1757-899X/252/1/012058.
[8] P.K. Das, Battery management in electric vehicles-current status and future trends, Batteries 10 (2024) 174, https://doi.org/10.3390/batteries10060174.
[9] B. Johansson, J. Johansson, The new attractive mine: 36 research areas for attractive workplaces in future deep metal mining, Int. J. Min. Miner. Eng. 5 (4) (2014) 350–361.
[10] B. FridleifssonI, R. Bertani, E. Huenges, J.W. Lund, A. Ragnarsson, L. Rybach, The possible role and contribution of geothermal energy to the mitigation of climate change, in: O. Hohmeyer, T. Trittin (Eds.), IPCC Scoping Meeting on Renewable Energy Sources, Citeseer, Luebeck, 2008, pp. 59–80.
[11] A. Kamyar, S.M. Aminossadati, C. Leonardi, A. Sasmito, Current developments and challenges of underground mine ventilation and cooling methods, in: N. Aziz, B. Kininmonth (Eds.), Proceedings of the 16th Coal Operators' Conference, Mining Engineering, University of Wollongong, Wollongong, 2016, pp. 277–287.
[12] Z.P. Cano, D. Banham, S. Ye, A. Hintennach, J. Lu, M. Fowler, Z. Chen, Batteries and fuel cells for emerging electric vehicle markets, Nat. Energy 3 (2018) 279–289, https://doi.org/10.1038/s41560-018-0108-1.
[13] S. Ahmed, I. Bloom, A.N. Jansen, T. Tanim, E.J. Dufek, A. Pesaran, A. Burnham, R.B. Carlson, F. Dias, K. Hardy, M. Keyser, C. Kreuzer, A. Markel, A. Meintz, C. Michelbacher, M. Mohanpurkar, P.A. Nelson, D.C. Robertson, D. Scoffield, M. Shirk, T. Stephens, R. Vijayagopal, J. Zhang, Enabling fast charging – a battery technology gap assessment, J. Power Sources 367 (2017) 250–262, https://doi.org/10.1016/j.jpowsour.2017.06.055.
[14] M. Keyser, A. Pesaran, Q. Li, S. Santhanagopalan, K. Smith, E. Wood, S. Ahmed, I. Bloom, E. Dufek, M. Shirk, A. Meintz, C. Kreuzer, C. Michelbacher, A. Burnham, T. Stephens, J. Francfort, B. Carlson, J. Zhang, R. Vijayagopal, K. Hardy, F. Dias, M. Mohanpurkar, D. Scoffield, A.N. Jansen, T. Tanim, A. Markel, Enabling fast charging – battery thermal considerations, J. Power Sources 367 (2017) 228–236, https://doi.org/10.1016/j.jpowsour.2017.07.009.
[15] R. Mathieu, O. Briat, P. Gyan, J.M. Vinassa, Comparison of the impact of fast charging on the cycle life of three lithium-ion cells under several parameters of charge protocol and temperatures, Appl. Energy 283 (2021) 116344, https://doi.org/10.1016/j.apenergy.2020.116344.
[16] Y. Yuan, Q. Ma, X. Zhang, F. Zhang, X. Song, H. Xin, G. Zhu, H. Zhang, Influence of cathode materials on thermal characteristics of lithium-ion batteries, Front. Chem. (2024), https://doi.org/10.3389/fchem.2024.1324840.
[17] Y. Li, Z. Zhou, L. Hu, M. Bai, L. Gao, Y. Li, X. Liu, Y. Li, Y. Song, Experimental studies of liquid immersion cooling for 18650 lithium-ion battery under different discharging conditions, Case Stud. Therm. Eng. 34 (2022), https://doi.org/10.1016/j.csite.2022.102034.
[18] Y.J. Guo, Z.L. Yang, K.L. Liu, Y.H. Zhang, W. Feng, A compact and optimized neural network approach for battery state-of-charge estimation of energy storage system, Energy 219 (2021) 1–10.
[19] B. Polnik, K. Kaczmarczyk, A. Niedworok, R. Baltes, E. Clausen, Energy recuperation as one of the factors improving the energy efficiency of mining battery locomotives, Manag. Syst. Prod. Eng. 28 (4) (2020) 253–258.
[20] Y. Miao, P. Hynan, A. Jouanne, A. Yokochi, Current Li-ion battery technologies in electric vehicles and opportunities for advancements, Energies 12 (2019) 1–20.
[21] M. Wentker, M. Greenwood, J. Leker, A bottom-up approach to lithium ion battery cost modeling with a focus on cathode active materials, Energies 12 (2019) 1–18.
[22] L. Ianniciello, P.H. Biwolé, P. Achard, Electric vehicles batteries thermal management systems employing phase change materials, J. Power Sources 378 (2018) 383–403, https://doi.org/10.1016/j.jpowsour.2017.12.071.

[23] Y. Yang, X. Huang, Z. Cao, G. Chen, Thermally conductive separator with hierarchical nano/microstructures for improving thermal management of batteries, Nano Energy 22 (2016) 301–309, https://doi.org/10.1016/j.nanoen.2016.01.026.
[24] V. Vishwakarma, C. Waghela, Z. Wei, R. Prasher, S.C. Nagpure, J. Li, F. Liu, C. Daniel, A. Jain, Heat transfer enhancement in a lithium-ion cell through improved material-level thermal transport, J. Power Sources 300 (2015) 123–131, https://doi.org/10.1016/j.jpowsour.2015.09.028.
[25] S. Gungor, G.D. Telli, S. Lorente, Characterizing Li-ion battery thermal behavior; a methodology when little information is available, Int. Commun. Heat Mass Tran. 148 (2023), https://doi.org/10.1016/j.icheatmasstransfer.2023.107076.
[26] M.J. McPherson, Subsurface Ventilation and Environmental Engineering, Springer, Dordrecht, 1993.
[27] S. Panchal, I. Dincer, M. Agelin-Chaab, R. Fraser, M. Fowler, Experimental and theoretical investigations of heat generation rates for a water cooled LiFePO4 battery, Int. J. Heat Mass Tran. 101 (2016), https://doi.org/10.1016/j.ijheatmasstransfer.2016.05.126.
[28] A. Nazari, S. Farhad, Heat generation in lithium-ion batteries with different nominal capacities and chemistries, Appl. Therm. Eng. (2017), https://doi.org/10.1016/j.applthermaleng.2017.07.126.